REPORTS OF PRACTICAL ONCOLOGY AND RADIOTHERAPY 17 (2012) 339–346

Available online at www.sciencedirect.com

SciVerse ScienceDirect

journal homepage: http://www.elsevier.com/locate/rpor

Thermal and resonance neutrons generated by various electron and X-ray therapeutic beams from medical linacs installed in polish oncological centers

Adam Konefał[a,*], *Andrzej Orlef*[b], *Marcin Łaciak*[a,d], *Aleksander Ciba*[c], *Marek Szewczuk*[b]

[a] *Department of Nuclear Physics and its Applications, Institute of Physics, Silesian University, Katowice, Poland*
[b] *Department of Medical Physics, Center of Oncology, Gliwice Branch, Gliwice, Poland*
[c] *Radiotherapy Department of the Stanisław Leszczyński Memorial Hospital, Katowice, Poland*
[d] *Institute of Occupational Medicine and Environmental Health, Sosnowiec, Poland*

ARTICLE INFO

Article history:
Received 5 October 2011
Received in revised form
24 April 2012
Accepted 14 June 2012

Keywords:
Thermal/resonance neutrons
Induce radioactivity
Medical linacs

ABSTRACT

Background: High-energy photon and electron therapeutic beams generated in medical linear accelerators can cause the electronuclear and photonuclear reactions in which neutrons with a broad energy spectrum are produced. A low-energy component of this neutron radiation induces simple capture reactions from which various radioisotopes originate and in which the radioactivity of a linac head and various objects in the treatment room appear.
Aim: The aim of this paper is to present the results of the thermal/resonance neutron fluence measurements during therapeutic beam emission and exemplary spectra of gamma radiation emitted by medical linac components activated in neutron reactions for four X-ray beams and for four electron beams generated by various manufacturers' accelerators installed in typical concrete bunkers in Polish oncological centers.
Materials and methods: The measurements of neutron fluence were performed with the use of the induced activity method, whereas the spectra of gamma radiation from decays of the resulting radioisotopes were measured by means of a portable high-purity germanium detector set for field spectroscopy.
Results: The fluence of thermal neutrons as well as resonance neutrons connected with the emission of a 20 MV X-ray beam is $\sim 10^6$ neutrons/cm^2 per 1 Gy of a dose in water at a reference depth. It is about one order of magnitude greater than that for the 15 MV X-ray beams and about two orders of magnitude greater than for the 18–22 MeV electron beams regardless of the type of an accelerator.
Conclusion: The thermal as well as resonance neutron fluence depends strongly on the type and the nominal potential of a therapeutic beam. It is greater for X-ray beams than for electrons. The accelerator accessories and other large objects should not be stored in a treatment room during high-energy therapeutic beam emission to avoid their activation caused by thermal and resonance neutrons. Half-lives of the radioisotopes originating from the simple capture reaction (n,γ) (from minutes to hours) are long enough to accumulate radioactivity of components of the accelerator head. The radiation emitted by induced radioisotopes causes the additional doses to staff operating the accelerators.

* *Corresponding author*. Tel.: +48 503830026.
E-mail address: adam.konefal@us.edu.pl (A. Konefał).

1507-1367/$ – see front matter © 2012 Greater Poland Cancer Centre. Published by Elsevier Urban & Partner Sp. z o.o. All rights reserved.
http://dx.doi.org/10.1016/j.rpor.2012.06.004

1. Background

High-energy photons and electrons used in radiotherapy can cause nuclear reactions (i.e. electronuclear and photonuclear reactions[1–4]) in which neutron radiation is produced. This problem was investigated by many authors.[5–19] The resulting neutrons have a broad energy spectrum with mean energy of several hundred keV.[5–9] Significant contribution to the spectrum is given by thermal and resonance neutrons.[10–12] These low-energy neutrons come into being as a result of a slow-down processes (elastic scattering, mainly) of neutrons produced in the above mentioned reactions. The neutrons are slowed down mainly in walls, floor and ceiling of a treatment facility. The thermal and resonance neutrons can cause simple capture reactions from which various radioisotopes originate and in which the radioactivity of air, linac head and various objects in the treatment room appear. The main sources of neutrons are large components of linac head[13] i.e. collimators of the beam, a flattening filter, a target in the case of X-ray beams and, additionally, scattered foils instead of a flattening filter in the case of electron beams. The resulting neutrons can travel through a treatment room and a maze.[8] Thus, simple capture reactions can take place in the whole treatment facility. A comprehensive knowledge of the nuclear reactions and radioisotopes induced during emission of therapeutic beams generated by medical linacs was presented in many papers.[14–21]

2. Aim

The main aim of this paper is to present the results of measurements of the thermal and resonance neutron fluence in the vicinity of a medical linac during emission of various high-energy therapeutic beams. Additionally, exemplary spectra of gamma radiation emitted by medical linac components activated in neutron reactions are shown. The purpose of this part of the study was to identify gamma emitters induced in neutron reactions in linac accessory during emission of high-energy photon/electron therapeutic beams. The presented investigations were carried out for four various therapeutic electron beams and for four X-ray beams generated by three various manufacturers' medical linacs installed in typical concrete bunkers in three Polish oncological centers: the Center of Oncology in Gliwice, the Stanisław Leszczyński Memorial Hospital in Katowice and the Greater Poland Cancer Centre in Poznań.

3. Materials and methods

3.1. *Measurements of the thermal and resonance neutron fluence*

The measurements of the thermal and resonance neutron fluence were performed with the use of the induced activity method. This method uses the dependence between the indium foil activity caused by thermal/resonance neutrons and the thermal/resonance neutron fluence. The neutron activation detectors were indium foils (^{115}In isotope) in the shape of a circle with the radius of 0.75 cm. The foil superficial density was in the range from 98 to 110 mg/cm^2. Isotope ^{115}In is characterized by a relatively high cross section of 160 b[22] for a simple thermal neutron capture reaction. It also has a high resonance of about 28,000 b[23] at 1.45 eV and a number of lower resonances in the 3.5 eV to 1 keV range for the above-mentioned reaction, yielding the resonance activation integral of 2700 b.[24]

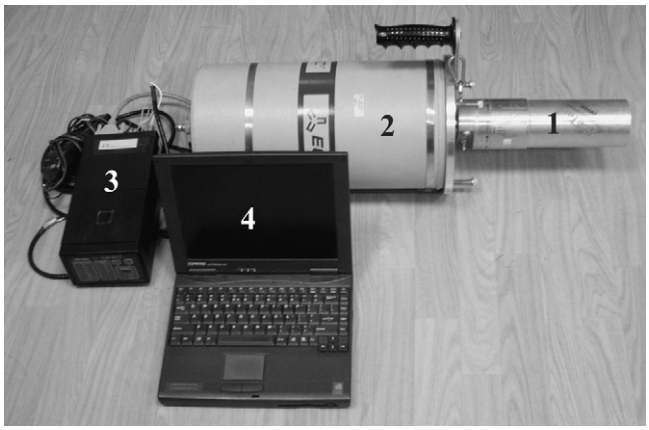

Fig. 1 – The view of the detection system with a high-purity germanium detector by ORTEC (1 – the aluminum shield of the germanium crystal, 2 – container with liquid nitrogen, 3 – electronic modules – multichannel analyzer, amplifier, etc., 4 – laptop).

The measurement of the thermal/resonance fluence consisted of two stages. In the first stage, the indium foil was placed at a chosen location in the neutron field induced by a therapeutic beam inside a treatment room. The indium foil was activated by a capture of neutrons. The thermal and resonance neutrons activate the indium according to the following reaction:

$$^{115}_{49}\mathrm{In} + {}^{1}_{0}n \rightarrow {}^{116m}_{49}\mathrm{In}\ (\text{unstable, half-life}\ T_{1/2} = 54.21\ \text{m})$$

followed by radioactive decay. The unstable state ^{116m}In disintegrates by β^- decay into the exited state ^{116}Sn*. Deexcitation of this state gives gammas. In the second stage, the activated foil was removed to the operator room after the therapeutic beam emission and it was located on the surface of the germanium detector shield to measure the indium foil activity. In the presented investigation, the detection system with the high-purity germanium detector by ORTEC (Fig. 1) was applied to measure the activity of the foil on the basis of a measurement of a spectrum of gammas emitted by the activated indium. In the presented investigation, the foil activity was determined by a net count area *NCA* of the peak at 1293.54 keV (Fig. 3), using the calibration factor *K*. The factor *K* was defined as a ratio of the activity of the calibration source ^{60}Co to net count area of the peak at 1332.50 keV in the gamma energy spectrum emitted by the ^{60}Co source used for the calibration. The energy of 1332.50 keV is close to 1293.54 keV from gammas emitted by the activated indium foil. The calibration source was in the same shape and it had the same surface as the applied indium foils.

The cadmium cover method was applied to separate the thermal neutron fluence and the resonance neutron fluence. Each measurement of the neutron fluence was performed twice: first by the use of the indium foil placed in a 1 mm thick cadmium shield, and then after the decay of the excited nuclei but without the shield. The cadmium shield absorbs almost all thermal neutrons but it lets through most of resonance ones. Thus, the total activity of the indium foil covered by cadmium is induced by resonance neutrons. However, a part of the resonance neutrons is absorbed in the cadmium layer. A correction for this absorption needs to be applied. For this purpose, the correction factor F_{Cd} was applied. F_{Cd} depends on a kind and a superficial density of a foil material used as well as a thickness of the cadmium layer.[25] It was 1.13 for the applied indium foil and the cadmium shield. The indium foil activity A_{res} caused by resonance neutrons is a product of the activity of the foil that was in the cadmium shield during the measurement and the correction factor F_{Cd}. Thus, $A_{res} = NCA_{in\ Cd} \times K \times F_{Cd}$, where $NCA_{in\ Cd}$ is a net count area of the peak at 1293.54 keV in the spectrum of gammas emitted by the indium foil activated by resonance neutrons. The difference between the activity A_{tot} induced in the uncovered foil and the one induced in the foil shielded by cadmium (A_{res}), adjusted for the resonance neutron absorption in cadmium, provides information about the activity induced by thermal neutrons: $A_{ther} = A_{tot} - A_{res} = (NCA - NCA_{in\ Cd} \times F_{Cd}) \times K$.

The final dependence between the indium foil activity and the thermal/resonance neutron fluence, when the cadmium cover method is applied, can be expressed as follows:

$$\Phi_{ther} = \frac{A_{ther} W e^{\lambda t_m} t_p \lambda}{d_m S N_0 \sigma_{ther} (1 - e^{-\lambda t_n})(e^{-\lambda t_p} - 1)},$$

$$\Phi_{res} = \frac{A_{res} F_{Cd} W e^{\lambda t_m} t_p \lambda}{d_m S N_0 C (1 - e^{-\lambda t_n})(e^{-\lambda t_p} - 1)} \int_{0.4\,eV}^{100\,keV} \frac{dE}{E},$$

and

$$C = \int_{0.4\,eV}^{\infty} \frac{\sigma(E)}{E} dE - \text{the resonance activation integral,}$$

where Φ_{ther} (Φ_{res}) is the thermal (resonance) neutron fluence, A_{ther} (A_{res}) is the measured indium foil detector activity due to thermal (resonance) neutrons, t_p is the time of the measurement of the gamma spectrum from the disintegration of $^{116}Sn^*$ (usually 10 min), t_n is the time of exposure to neutron radiation, t_m is the time between the end of the neutron exposure and the beginning of the measurement of the gamma spectrum from the disintegration of $^{116}Sn^*$, d_m is the foil superficial density, σ_{ther} is the thermal neutron simple capture cross section, λ is the decay constant (0.012739 min^{-1} for ^{116m}In), F_{Cd} is the correction factor for the absorption of resonance neutrons in the cadmium shield, W is the atomic weight of material used as the neutron activation detector (^{115}In), S is the foil area (1.77 cm^2 for the used foils) and N_o is the Avogadro's number, E is the neutron energy.

The determined fluence values were normalized to the therapeutic beam dose D_{ref} in water at the reference depth. According to the recommendation of the dosimetry protocols[26,27] the reference depth is 10 cm for all considered X-ray beams, whereas in the case of electrons it depends on the beam energy (i.e. the reference depth is a depth of maximum dose). Due to the normalization, the presented values of the neutron fluence are independent of accelerator efficiency. The measurements of the thermal/resonance neutron fluence were performed for the 10 cm × 10 cm radiation field specified on a therapeutic couch surface. The indium foil was placed in the center of the radiation field on the surface of a therapeutic couch for SSD (Source Surface Distance) equal to 100 cm and on walls of the treatment room (Fig. 2) at about 1.0–1.4 m over the floor surface. The therapeutic beam dose was referred to the thermal/resonance fluence by a number of monitor units determining the amount of photon/electron radiation from a therapeutic beam emitted during the indium foil activation. The number of monitor units was determined by the use of an internal dosimetry system of linacs. 6000 monitor units were usually used for each activation (600 monitor units per minute – a maximal efficiency of accelerators, time of activation: 10 min). Each value of the thermal/resonance neutron fluence presented in this paper comes from averaged data for three or more measurements performed for one or two bunkers. All considered linacs were installed in bunkers with a similar construction. The bunkers consisted of a treatment room and a maze. The uncertainty in the determined thermal and resonance fluence did not exceed 20% when the foils were exposed to neutrons for 10 min, for the maximal efficiency of accelerators. The time of the foil activity measurement was 10 min. It was enough to determine net count area of the peak at 1293.54 keV with the accuracy of about 5%.

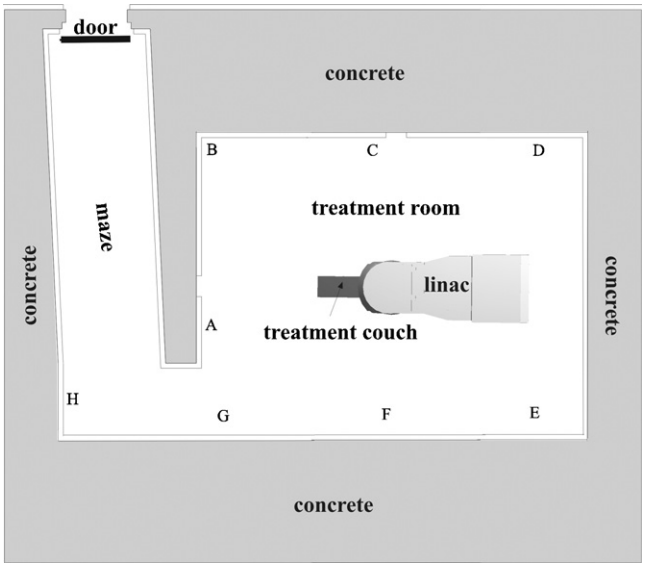

Fig. 2 – Scheme of the accelerator bunker with the denoted locations of the measurements of the thermal/resonance neutron fluence.

3.2. *Measurements of the energy spectra of gamma radiation from decays of the induced radioisotopes*

One of the basic methods used to identify radioisotopes originated from a treatment room is gamma spectroscopy. In the presented investigation, gamma spectroscopy was realized with the use of the ORTEC high-purity germanium detector

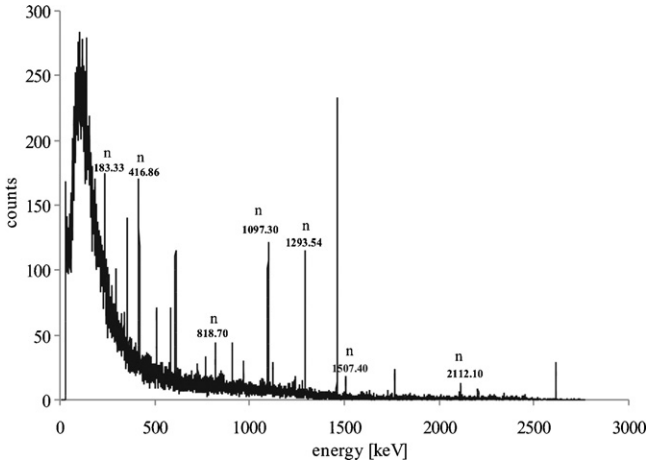

Fig. 3 – The exemplary gamma energy spectrum from deexcitation of $^{116}Sn^*$. The spectrum was measured by the use of the ORTEC gamma detection system with the high-purity germanium detector. During the neutron activation the foil was placed at the isocentre of the linac head rotation, thus it was simultaneously not only in the neutron field but also in the gamma/electron field. In connection of this the foil was activated by neutrons in the simple capture reactions as well by gammas in the photonuclear reactions or by electrons in electronuclear reactions. The peaks from the neutron activation are denoted by *n* and energy in keV is given.

applied usually for field spectrometry (Fig. 1). The detection system consisted of the above-mentioned detector connected to a MiniMCA177 multichannel analyzer installed in a PC computer (laptop). The work of the detector was operated by the M-1-B32 software. Such detection system is relatively small and can be easily displaced. The energy calibration was performed with the use of a set of commercial calibration sources: ^{22}Na, ^{54}Mn, ^{60}Co, ^{74}Se, ^{133}Ba, ^{137}Cs, and ^{241}Am. The same detection system was applied to measure the indium foil activity in the thermal/resonance neutron measurements. The details of gamma spectroscopy have been presented in many publications [see for example[28,29]]. Analysis of the measured spectra was based on the knowledge of materials applied in a construction of the considered linacs. The tables of isotopes edited by Firestone[30] were very useful for this analysis. The verification of the method used was carried out for natural samples, including uranium series.

4. Results

An exemplary gamma spectrum from the deexcitation of $^{116}Sn^*$, measured by the applied detection system is presented in Fig. 3. Such spectra were the basis of the induced activity method used for the determination of the indium foil activity in the presented investigations.

Comparison of the thermal/resonance neutron fluence values at the isocentre of the linac head rotation is shown in Table 1. The fluence of thermal neutrons as well as resonance neutrons connected with the emission of the 20 MV X-ray beam is about one order of magnitude greater than that for the 15 MV X-ray beams and about two orders of magnitude greater than for the considered electron beams, regardless of the type of an accelerator. In the case of the 15 MV X-ray beam emitted by the Elekta-Synergy linac, the thermal neutron fluence is approximately two times less than that for the 15 MV X-rays from the two remaining considered linacs. However, the resonance neutron fluence for the 15 MV X-ray beam from Elekta-Synergy is at the level of that of the Primus accelerators and two times less than in the case of 15 MV X-rays generated in Clinac-2300. In the case of electron beams emitted by Primus, the thermal neutron fluence is about two times greater than the resonance fluence. This tendency is opposite for the electron beams from Clinac-2300.

The distribution of the thermal/resonance neutron fluence in treatment rooms with Clinac-2300 and Primus is shown in Table 2. The thermal and resonance neutron fluence does not change significantly in the treatment rooms. It is the same order of magnitude in the vicinity of treatment room walls as at the isocentre of the linac head rotation for both considered accelerators. Thus, the accelerator accessories can be activated by neutrons even when they are not used but stored inside a treatment room during high-energy therapeutic beam emission.

The measured energy spectra of gammas emitted by chosen components of an accelerator head are presented in Figs. 4 and 5. The spectrum of gammas emitted by the activated isolated flattening filter used in Clinac-2300 working in the 15 MV mode is presented in Fig. 4. The gamma energy spectrum for the activated Clinac-2300 electron applicator forming a 10 cm × 10 cm radiation field is shown in Fig. 5.

The peak at 846.77 keV visible in the spectra in Fig. 4 as well as in Fig. 5 and the peak at 1810.77 keV present in the spectrum in Fig. 5 come from the decay of excited state $^{56}Fe^*$ being a consequence of simple capture reactions with ^{55}Mn – the only natural isotope of manganese (abundance given in the parenthesis in the reaction notation is equal to 100%):

$$^1_0n + {}^{55}_{25}\mathrm{Mn}(100\%) \rightarrow \gamma + {}^{56}_{25}\mathrm{Mn}.$$

The state of ^{56}Mn is unstable and disintegrates by emission of β^- radiation:

$$^{56}_{25}\mathrm{Mn} \underset{T_{1/2}=2.58\,\mathrm{h}}{\longrightarrow} \beta^- + {}^{56}_{26}\mathrm{Fe}^* \underset{T_{1/2}<6\,\mathrm{ps}}{\longrightarrow} {}^{56}_{26}\mathrm{Fe(stable)} + \gamma(846.77\,\mathrm{keV}, 1810.77\,\mathrm{keV}).$$

The maximum range of emitted electrons is 1256 cm in air and 1.6 cm in a biological tissue. The maximum ranges of electrons from the β^- decay in air and in a biological tissue inserted in this paper were estimated on the base of equivalent values of exposure constant given by Gostkowska.[33] The air density of 0.0013 g/cm^3 and the biological tissue density of 1 g/cm^3 were taken for the estimations of the electron ranges.

The peaks at 134.24 keV, 479.59 keV, 551.53 keV, 618.36 keV, 625.51 keV, 685.77 keV and 772.89 keV visible in the spectrum in Fig. 4 come from the decay of excited state $^{187}Re^*$ being a consequence of the simple capture reactions with ^{186}W:

$$^1_0n + {}^{186}_{74}\mathrm{W}(28.6\%) \rightarrow \gamma + {}^{187}_{74}\mathrm{W}.$$

Table 1 – The thermal (Φ_{ter}) and resonance (Φ_{res}) neutron fluence values at the isocenter of the linac head rotation, normalized to a dose D_{ref} in water at the reference depth. The presented values were determined with the use of the induced activity method. The measurement was performed three or more times in each measurement point. The uncertainty in the presented data in the thermal/resonance neutron measurements do not exceed 20%.

Beam	Accelerator	Φ_{ter}/D_{ref} [cm^{-2} Gy^{-1}]	Φ_{res}/D_{ref} [cm^{-2} Gy^{-1}]
15 MV X-rays	[c]Clinac-2300	3.0×10^5	2.7×10^5
15 MV X-rays	[a]Primus	3.7×10^5	1.6×10^5
15 MV X-rays	[a]Elekta-Synergy	1.4×10^5	1.4×10^5
20 MV X-rays	[b]Clinac-2300	1.5×10^6	1.2×10^6
18 MeV electrons	[b]Clinac-2300	0.7×10^4	1.4×10^4
18 MeV electrons	[a]Primus	1.1×10^4	0.6×10^4
21 MeV electrons	[a]Primus	1.9×10^4	0.8×10^4
22 MeV electrons	[b]Clinac-2300	1.0×10^4	2.0×10^4

[a] Installed in Hospital – Memorial Stanisław Leszczyński in Katowice.
[b] Installed in Center of Oncology in Gliwice.
[c] Installed in Greater Poland Cancer Centre in Poznań.

Table 2 – The thermal (Φ_{ter}) and resonance (Φ_{res}) neutron fluence values at the chosen locations in the treatment room (see Fig. 3) during emission of the 15 MV and 20 MV X-ray beams generated by [a]Primus and [b]Clinac-2300, respectively. Otherwise as in Table 1.

Location	15 MV, Primus		20 MV, Clinac-2300	
	Φ_{ter}/D_{ref} [cm^{-2} Gy^{-1}]	Φ_{res}/D_{ref} [cm^{-2} Gy^{-1}]	Φ_{ter}/D_{ref} [cm^{-2} Gy^{-1}]	Φ_{res}/D_{ref} [cm^{-2} Gy^{-1}]
A	3.2×10^5	1.0×10^5	1.4×10^6	1.0×10^6
B	2.5×10^5	0.4×10^5	2.1×10^6	1.5×10^6
C	4.1×10^5	0.8×10^5	2.1×10^6	1.5×10^6
D	2.9×10^5	1.1×10^5	1.6×10^6	1.1×10^6
E	2.9×10^5	0.5×10^5	1.6×10^6	1.1×10^6
F	3.9×10^5	1.5×10^5	2.2×10^6	1.5×10^6
G	2.8×10^5	0.4×10^5	1.2×10^6	0.9×10^6
H	2.1×10^5	0.3×10^5	0.1×10^6	0.1×10^6

[a] Installed in Hospital – Memorial Stanisław Leszczyński in Katowice.
[b] Installed in Center of Oncology in Gliwice.

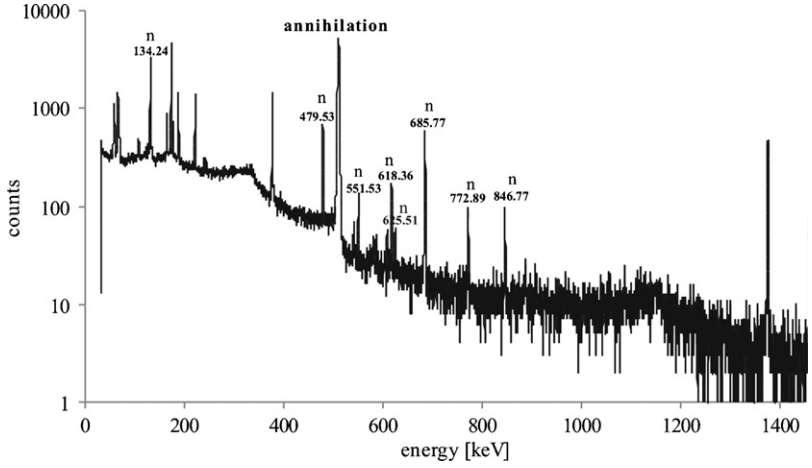

Fig. 4 – The energy spectrum of gamma radiation measured during decays of radioisotopes induced in the flattening filter of Clinac-2300 working in the 15 MV mode. The spectrum was measured with the use of an ORTEC detection system with the high-purity germanium detector (see Fig. 1). The peaks from radioisotopes induced in neutron reactions are denoted by *n* and additionally energy in keV was given for each peak. The remaining peaks come mainly from photonuclear reactions. The flattening filter was located at the isocentre of the linac head rotation on a treatment couch during emission of the therapeutic beam. The spectrum was measured immediately after removing the filter from the beam.

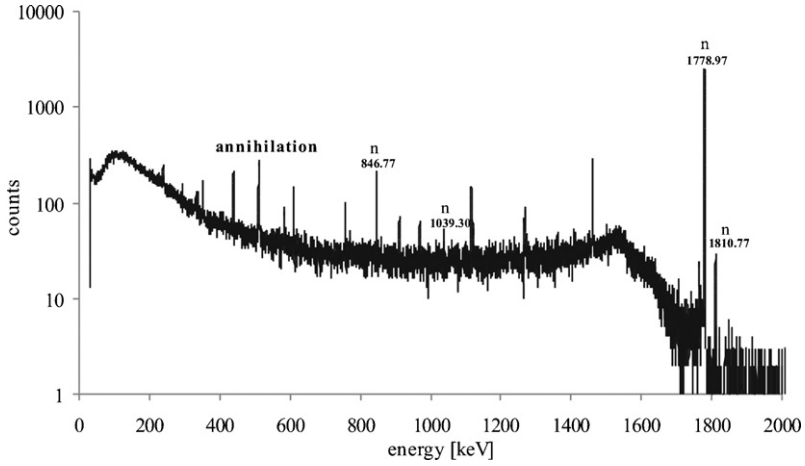

Fig. 5 – The energy spectrum of gamma radiation measured during decays of radioisotopes induced in the electron applicator forming a radiation field of 10 cm × 10 cm for Clinac-2300. The electron applicator was stored outside the therapeutic beam in the corner of a treatment room during emission of therapeutic beams. The spectrum was measured immediately after emission of the 15 MV X-ray beam. Otherwise as in Fig. 4.

The appropriate decay of the unstable state of ^{187}W can be written as:

$$^{187}_{74}\mathrm{W} \underset{T_{1/2}=23.72\,\mathrm{h}}{\longrightarrow} \beta^- + {}^{187}_{75}\mathrm{Re}^* \underset{T_{1/2}<1\,\mathrm{ms}}{\longrightarrow} {}^{187}_{75}\mathrm{Re(stable)} + \gamma$$

$$\times\,(134.24, 473.59, 551.53, 618.36, 625.51, 685.77, 772.89\,\text{in keV})$$

The maximum range of electrons from the β^- decay of ^{187}W is equal to 429 cm in air and 0.6 cm in a biological tissue. The remaining isotopes of tungsten can change into stable isotopes or into radioisotopes which do not emit gammas. The reaction ^{186}W$(n,\gamma)^{187}$W is characterized by the neutron thermal cross section of 37.9 b,[32] the greatest of all natural tungsten isotopes, and by a relatively large resonance activation integral of 355 b.[24]

The high peak at 1778.97 keV visible in the energy spectrum of gammas emitted by the electron applicator (Fig. 5) is a result of the activation of aluminum ^{27}Al with abundance of 100%:

$$^{1}_{0}n + {}^{27}_{13}\mathrm{Al(100\%)} \rightarrow \gamma + {}^{28}_{14}\mathrm{Al},$$

followed by the radioactive decay:

$$^{28}_{13}\mathrm{Al} \underset{T_{1/2}=2.24\,\mathrm{m}}{\longrightarrow} \beta^- + {}^{28}_{14}\mathrm{Si}^* \underset{T_{1/2}<1\,\mathrm{ps}}{\longrightarrow} {}^{28}_{14}\mathrm{Si(stable)} + \gamma(1778.97\,\mathrm{keV}).$$

The cross section of the reaction ^{27}Al$(n,\gamma)^{28}$Al is about 0.231 b at the thermal energy.[32] One greater resonance of 4.685 b appears at 5904 keV.[24] The maximum range of electrons from the β^- decay of ^{28}Al is equal to 1265 cm in air and 1.6 cm in a biological tissue.

The peak at 1039.3 keV present in the spectrum shown in Fig. 5 is a result of the following simple capture reaction:

$$^{1}_{0}n + {}^{65}_{29}\mathrm{Cu(30.8\%)} \rightarrow \gamma + {}^{66}_{29}\mathrm{Cu},$$

followed by the decay of the nucleus of ^{66}Cu:

$$^{66}_{29}\mathrm{Cu} \underset{T_{1/2}=5.1\,\mathrm{m}}{\longrightarrow} \beta^- + {}^{66}_{30}\mathrm{Zn}^* \underset{T_{1/2}<1.65\,\mathrm{ps}}{\longrightarrow} {}^{66}_{30}\mathrm{Zn(stable)} + \gamma(1039.3\,\mathrm{keV}).$$

The neutron thermal cross section of ^{65}Cu$(n,\gamma)^{66}$Cu is about 2.17 b.[32] The maximum range of electrons from the β^- decay of ^{66}Cu is equal to 1126 cm in air and 1.5 cm in a biological tissue. Second natural isotope of copper ^{63}Cu with abundance of 69.17% changes into ^{64}Cu disintegrating by beta decay or electron capture. In this case, the emission of gammas (invisible in the measured spectrum) accompanies only every 200th decay.

5. Discussion

The presented values of the thermal fluence connected with the emission of the X-ray beams are in a good agreement with results obtained by Gudowska and Brahme[31] for the various accelerators' X-ray beams with the nominal potential nearing the considered ones. Gudowska and Brahme applied the indium foil as well as the fission chamber with ^{235}U for the thermal neutron measurements. The thermal neutron fluences measured during the emission of a15 MV X-ray beam are very close to that obtained by Liu at al.[34] with the use of activation of the indium foil for Clinac-2100 working in the 15 MV X-ray mode. Moreover, the fluences of thermal/resonance neutrons produced during the emission of the considered 20 MV X-rays agree with those derived by our Monte Carlo calculations presented in Ref.[8]

Using the neutron dose equivalent conversion factors given in Ref.[35] effective doses from thermal and resonance neutrons can be estimated on the basis of the measured neutron fluences. In the case of all considered therapeutic X-ray beams, the thermal and resonance neutron effective doses obtained by patients do not exceed 50 μSv per 1 Gy of therapeutic X-ray dose. In the case of the considered therapeutic electron beams, the thermal and resonance neutron effective doses are about two orders of magnitude less than those for the X-rays. Thus, the thermal/resonance neutron doses to patients

treated by high-energy X-ray/electron beams can be neglected in considerations of peripheral doses to patients. As shown in the investigations in Refs.,[6,31] the main contribution to neutron doses to patients comes from fast neutrons. It is caused by two factors. Firstly, fast neutron fluence is about one order of magnitude greater than that for thermal/resonance neutrons. Secondly, the neutron dose equivalent conversion factors[35] for fast neutrons are about 10 times greater than for neutrons with thermal and resonance energies. In general, in the case of high-energy therapeutic X-rays, the main contribution to peripheral doses to patients is given by fast neutrons and photons from scattering of the primary beam.[36] Significant consequence of the thermal/resonance neutron existence is the production of radioisotopes emitting a penetrative gamma radiation and electrons with relatively long ranges for many materials applied in the accelerator head constructions, such as manganese, tungsten, aluminum, and copper.

The manganese ^{55}Mn is a component of both considered accelerator accessories. In general, it is one of the fundamental components of stainless steel applied in the construction of various parts of medical accelerators. This isotope is easily activated by low-energy neutrons, because it has a large cross section for the neutron capture reaction, i.e. the thermal neutron capture cross section is 13.2 b[32] and the resonance activation integral is 15.7 b,[24] with the high resonance peak occurring at 337 eV.[32]

Constructions of heads of the contemporary medical linacs are characterized by a great amount of tungsten. The considered flattening filter of Clinac-2300 working in the 15 MV mode is mainly made of tungsten. There are five natural stable isotopes of tungsten (abundances in the parenthesis): ^{180}W (0.1%), ^{182}W (26.3%), ^{183}W (14.3%), ^{184}W (30.7%) and ^{186}W (28.6%). Three of them (i.e. ^{180}W, ^{184}W and ^{186}W) can be changed into radioisotopes in the simple capture reactions. Two of them (i.e. ^{182}W and ^{183}W) change into stable nuclei when a neutron is captured. The neutron capture reaction with ^{184}W produces ^{185}W – a β^- emitter undetected in gamma spectroscopy, whereas the radioisotope of ^{181}W is not visible in the presented spectra because ^{180}W has too small abundance.

The large intensity of the peak at 1778.97 keV visible in Fig. 5 is a consequence of a relatively short half-life radioisotope ^{28}Al and a large amount of aluminum in the construction of the electron applicator. The wires connected to a push sensor on the bottom of the electron applicator are made of copper. The amount of this isotope is relatively small in the construction of the considered electron applicator which results in a low intensity peak at 1039.3 keV in spite of a relatively short half-life.

In general, radioisotopes identified in the presented investigations were also observed in other components of medical accelerators.[15–21] As shown in the presented investigations, the level of induced radiation and the thermal and resonance neutrons depends mainly on the kind and nominal potential of therapeutic beams. The type of a linac has less influence on those phenomena. It is caused by the fact that the cross sections of the (γ,n) and $(e,e'n)$ reactions depend on the energy of gammas and electrons [see for example[21]].

6. Conclusions

1. In general, the thermal as well as resonance neutron fluence depends strongly on the type of the therapeutic beam. It is greater for X-rays beams than for electrons.
2. In the case of therapeutic X-rays beams, the thermal and resonance neutron fluence is greater for beams with a higher nominal potential (the dependence of the neutron fluence upon a type of a linac is of lower significance).
3. The accelerator accessories and other massive objects should not be stored close to a treatment room during high-energy therapeutic beam emission, to avoid their activation caused by the thermal and resonance neutrons. To reduce the activation of the accelerator components, all replaceable massive accessories of a linac should be stored outside the bunker.
4. Neutrons with thermal and resonance energies cause the simple capture reaction (n,γ) in which undesirable radioisotopes originated. Half-lives of these radioisotopes range from minutes to hours. Such half-lives are long enough for components of the accelerator head to accumulate radioactivity. To reduce the radioactivity accumulation, longer lasting emission of high-energy X-ray beams should be avoided if possible.
5. The radiation emitted by induced radioisotopes causes additional doses to staff operating accelerators. The values of these doses depend mainly on time of emission of high-energy X-ray beams, intervals between these emissions and time a person spends close to an accelerator head.

Conflict of interest

There is no conflicts of interest.

Financial disclosure

The study was partially supported by the Silesian University.

Acknowledgements

The authors of this paper are very grateful to young physicists from the Greater Poland Cancer Centre in Poznań for isolating the flattening filter used in Clinac-2300 with the 15 MV X-ray beam mode.

REFERENCES

1. Berman BL, Dietrich SS, editors. Atlas of photonuclear cross sections obtained with monoenergetic photons. *At Data Nucl Data Tables* 1998;**38**(2):199–338.
2. Giacri ML, Chadwick MB, Ridikas D, Young PG, Wilson WB. Photonuclear physics in radiation transport III: actinide cross-sections and spectra. *Nucl Sci Eng* 2006;**153**:1.
3. Ridikas D, Giacri ML, Chadwick MB, et al. Status of the photonuclear activation file: reaction cross-section. Fission fragments and delayed neutrons. *Nucl Instrum Methods Phys Res A* 2006;**562**:710–3.

4. Scott MB, Hanson AO, Kerst DW. Electro- and photo-disintegration cross sections of ^{63}Cu. *Physiol Rev* 1955;**100**:205.
5. Facure A, Falcao RC, Silva AX, Crispim VR, Vitorelli JC. A study of neutron spectra from medical linear accelerators. *Appl Radiat Isot* 2005;**62**:69–72.
6. Konefał A, Polaczek-Grelik K, Orlef A, Maniakowski Z, Zipper W. Background neutron radiation in the vicinity of Varian Clinac-2300 medical accelerator working in the 20 MV mode. *Pol J Environ Stud* 2006;**15**(4A):177–80.
7. Esposito A, Bedogni R, Lembo L, Morelli M. Determination of the neutron spectra around an 18 MV medical LINAC with a passive Bonner sphere spectrometer based on gold foils and TLD pairs. *Radiat Meas* 2008;**43**:1038–43.
8. Konefał A, Orlef A, Zipper W, Dorda J, Łobodziec W. Undesired neutron radiation generated by biomedical accelerators during high-energy X-ray and electron beam emission. *Pol J Med Phys Eng* 2001;**7**(4):291–304.
9. Amgarou K, Lacoste V, Martin A. Experimental characterization of the neutron spectra generated by a high-energy clinical LINAC. *Nucl Instrum Methods Phys Res A* 2011;**629**:329–36.
10. Vega-Carrillo HR, Baltazar-Raigosa A. Photoneutron spectra around an 18 MV LINAC. *J Radioanal Nucl Chem* 2011;**287**:323–7.
11. Konefał A, Dybek M, Zipper W, Łobodziec W, Szczucka K. Thermal and epithermal neutrons in the vicinity of the Primus Siemens biomedical accelerator. *Nukleonika* 2005;**50**(2):73–81.
12. Konefał A, Orlef A, Dybek M, Maniakowski Z, Polaczek-Grelik K, Zipper W. Correlation between radioactivity induced inside the treatment room and the undesirable thermal/resonance neutron radiation produced by linac. *Phys Med* 2008;**24**:212–8.
13. Mao XS, Kase KR, Liu JC, Nelson WR, Kleck JH, Johnsen S. Neutron sources in the Varian Clinac 2100C/2300C medical accelerator calculated by the EGS4 code. *Health Phys* 1997;**72**(4):524–9.
14. McGinley PH, White TA. Air activation produced by high-energy medical accelerators. *Med Phys* 1983;**10**(6):796–800.
15. Naseri A, Mesbahi A. A review on photoneutrons characteristics in radiation therapy with high energy photon beams. *Rep Pract Oncol Radiother* 2010;**15**:138–44.
16. Guo S, Ziemer PL. Health physics aspects of neutron activated components in a linear accelerator. *Health Phys* 2004;**2**(Suppl. 86):S94–102.
17. Evdokimoff V, Willins J, Richter H. Induced radioactive potential for a medical accelerator. *Health Phys Operat Radiat Safety* 2005;**5**(Suppl. 83):S68–70.
18. Fisher HW, Tabot B, Poppe B. Activation processes in medical linear accelerators and spatial distribution of activation products. *Phys Med Biol* 2006;**51**:N461–6.
19. Fisher HW, Tabot B, Poppe B. Activation products in medical linear accelerators. In: *IRPA second European congress. Session: RP in medicine*. 2006.
20. Konefał A, Polaczek-Grelik K, Zipper W. Undesirable nuclear reactions and induced radioactivity as a result of the use of the high-energy therapeutic beams generated by medical linacs. *Radiat Prot Dosim* 2008;**128**(2):133–45.
21. Konefał A. *Undesirable radioisotopes induced by therapeutic beams from medical linear accelerators. Chapter in: radioisotopes – application in bio – medical science*. INTECH Open Access Publisher; 2011, ISBN 978-953-307-748-2. p. 127–50.
22. Beckurc K, Wirtc K, editors. *Niejtronnaja fizika*. Moscow: Atomizdat; 1968.
23. Price WJ. *Nuclear radiation detection*. USA: McGraw-Hill Book Company; 1964.
24. Macklin RL, Pomerance HS. Resonance capture integrals. In: *Proceedings of the first international conference in peaceful uses of atomic energy, vol. 5*. 1956. p. 96.
25. Tittle WC. Slow neutron detection by foils – II. *Nucleonics* 1951;**9**:60.
26. IAEA. *Absorbed dose determination in photon and electron beams*. Vienna: International Atomic Energy Agency; 1987.
27. IAEA. *Absorbed dose determination in External beam radiotherapy: an international code of practice for dosimetry based on standards of absorbed dose to water*. Vienna: International Atomic Energy Agency; 2000.
28. International Commission on Radiation Units and Measurements. Gamma-Ray Spectrometry in the Environment. ICRU Report 53. Maryland; December 1994.
29. International Electrotechnical Commission. In situ photon spectrometry using a germanium detector for measuring discrete radionuclides in the environment. IEC 209 FDIS; May 1992.
30. Firestone RB, editor. *Table of isotopes*. 8th ed. University of California: Lawrence Berkeley National Laboratory; 1996, version 1.0.
31. Gudowska J, Brahme A. Neutron radiation from high-energy X-ray medical accelerators. *Nukleonika* 1996;**41**(2):105–18.
32. National Nuclear Data Center. Brookhaven National Laboratory. Web retrieval system. http://www.nndc.bnl.gov/sigma/search.jsp.
33. Gostkowska B. Ochrona radiologiczna. Wielkości. jednostki i obliczenia. Centralne Laboratorium Ochrony Radiologicznej. Warsaw (in Polish); 2005.
34. Liu W-S, Changlai S-P, Pan L-K, Tseng H-C, Chen C-Y. Thermal neutron fluence in a treatment room with a Varian linear accelerator at a medical university hospital. *Radiat Phys Chem* 2011;**80**:917–22.
35. ICRP. Conversion Coefficient for use in Radiological Protection against External Radiation. Publication 74; 1971.
36. Kry FS, Mohammad S, Followill DS, et al. Out-of-field photon and neutron dose equivalents from step-and-shoot intensity-modulated radiation therapy. *Int J Radiat Oncol Biol Phys* 2005;**62**(4):1204–16.